Spatial dispersion in atom-surface quantum friction

D. Reiche, D. A. R. Dalvit, K. Busch, and F. Intravaia

Phys. Rev. B **95**, 155448 — Published 27 April 2017

DOI: 10.1103/PhysRevB.95.155448

Spatial dispersion in atom-surface quantum friction

D. Reiche,[1,2] D. A. R. Dalvit,[3] K. Busch,[1,2] and F. Intravaia[2]

[1] *Humboldt-Universität zu Berlin, Institut für Physik, AG Theoretische Optik & Photonik, 12489 Berlin, Germany*

[2] *Max-Born-Institut, 12489 Berlin, Germany*

[3] *Theoretical Division, MS B213, Los Alamos National Laboratory, Los Alamos, NM 87545, USA*

We investigate the influence of spatial dispersion on atom-surface quantum friction. We show that for atom-surface separations shorter than the carrier's mean free path within the material, the frictional force can be several orders of magnitude larger than that predicted by local optics. In addition, when taking into account spatial dispersion effects, we show that the commonly used local thermal equilibrium approximation underestimates by approximately 95% the drag force, obtained by employing the recently reported nonequilibrium fluctuation-dissipation relation for quantum friction. Unlike the treatment based on local optics, spatial dispersion in conjunction with corrections to local thermal equilibrium not only change the magnitude but also the distance scaling of quantum friction.

I. INTRODUCTION

Quantum fluctuations give rise to numerous fascinating physical effects, especially on sub-micrometer scales. Some of these phenomena have been extensively studied and carefully measured, thus demonstrating their relevance for both fundamental physics and future technologies [1, 2]. Recently, there has been a renewed interest in fluctuation-induced interactions in nonequilibrium systems. A prominent example is quantum friction [3, 4], the quantum drag force between two uncharged, polarizable objects in relative motion. A large part of the existing literature on quantum friction considers an atom (or some other microscopic object) moving in front of a flat surface, where the corresponding material is modeled using local optics, i.e. assuming an optical response described by a permittivity that only depends on frequency. [5–14]. Within the assumption of local optics, several conceptual questions have been previously addressed, including the functional dependence of the frictional force on the atom's velocity [11, 14, 15], the impact of non-Markovian effects [16], and even the relevance of nonequilibrium correlations [17].

At short distances from the surface, however, a local description of the material becomes inadequate. Earlier works [18–21] have already shown that using a *nonlocal* description can lead to corrections to equilibrium dispersion forces [22]. Nonlocality is to be understood in the sense that spatial dispersion is included in an optical response, i.e. the material's permittivity depends on both frequency and wavevector. Also, in the case of surface-surface quantum friction, different material models that include spatial dispersion have been used to describe the drag force [4, 23–27]. The authors of these works have demonstrated that for short distances spatial nonlocality can lead to an enhancement of the force relative to the case of a local material model [23–26]. These works, however, have resorted to the so-called local thermal equilibrium (LTE) approximation, where it is assumed that the subsystems in relative motion are at equilibrium with their immediate surroundings. Such a procedure allows to utilize results of equilibrium thermodynamics, like the fluctuation-dissipation theorem (FDT) [28], but neglects the contribution due to nonequilibrium correlations [17, 29]. In fact, recent work has shown that the LTE approximation is not well justified for atom-surface quantum friction and underestimates the magnitude of the drag force [17]. Since the LTE approximation relies on a short correlation length of the fluctuations that mediate the interaction, one can expect that, when spatial dispersion is taken into account, the deviation from the LTE result is even larger than in the local optics treatment.

In this work, we study effects of spatial dispersion in atom-surface quantum friction and compare the results obtained using the LTE approximation with those obtained using a full nonequilibrium approach. We show that spatial dispersion enhances the failure of the LTE approximation, resulting in a 95% deviation from the full nonequilibrium result compared to the 80% deviation previously reported within local optics [17]. In addition, we show that the inclusion of spatial nonlocality strongly affects the functional distance dependence of the frictional force in the low-velocity limit. In contrast to the local optics case, where both the LTE and the full nonequilibrium approach predict the same distance scaling law for the quantum frictional force, their distance behaviors are different in the presence of spatial dispersion.

II. ATOM-SURFACE QUANTUM FRICTION

Consider an atom driven by an external force and moving with non-relativistic velocity ($|\mathbf{v}| \ll c$) at constant height $z_a > 0$ parallel to a conducting isotropic half-space. The atom is modeled as an electric dipole, described by the quantum operator $\hat{\mathbf{d}}(t)$. Due to the interaction of the atom with the surrounding quantum electromagnetic field a drag force will progressively balance the external drive until the system reaches a nonequilibrium steady state, where the motion continues with

constant velocity. Dissipation in the material gives rise to a nonzero memory time, such that in the nonequilibrium steady state we can ignore the transient acceleration process and assume that the atom has reached the trajectory $\mathbf{r}_a(t) = \mathbf{r}_0 + v_x t\mathbf{x}$ [15, 16] (we assume that the motion is along the x-direction). In an earlier work [16], we have shown that the zero-temperature drag force felt by the atom in such a situation can be written as

$$F = -2\int_0^\infty d\omega \int \frac{d^2\mathbf{p}}{(2\pi)^2} \times p_x \mathrm{tr}\left[\underline{S}_R(p_x v_x - \omega, v_x)\cdot \underline{G}^s_I(\mathbf{p}, z_a, \omega)\right], \quad (1)$$

where $p = |\mathbf{p}| = \sqrt{p_x^2 + p_y^2}$ is the parallel component of the three-dimensional electromagnetic wave vector $\mathbf{k} = p_x\mathbf{x} + p_y\mathbf{y} + q\mathbf{z}$ [30]. For symmetry reasons, the frictional force is only along the direction of the motion, i.e. $\mathbf{F} = F\mathbf{x}$. Quantum friction is determined by the velocity-dependent nonequilibrium power spectrum tensor of the dipole fluctuations, $\underline{S}(\omega, v_x)$, and by the Fourier transform (in time and xy-direction) of the electromagnetic surface Green tensor, $\underline{G}(\mathbf{p}, z_a, \omega)$. In Eq. (1) and in the remainder of the paper the subscript R (I) denotes the real (imaginary) part of an expression and the superscript s gives the symmetric part of a tensor [30]. The Green tensor is given by the sum of a vacuum contribution $\underline{G}_0$ and a scattering contribution $\underline{g}$. Because of Lorentz invariance, only the latter contributes to the final result [13, 31, 32]. In all this work we focus on atom-surface distances within the surface's near-field region. In this case the part of the scattered Green tensor relevant to quantum friction [30] is

$$\underline{g}^s(\mathbf{p}, z_a, \omega) = \frac{p e^{-2z_a p}}{2\epsilon_0} r(\omega, p)\left[\frac{p_x^2}{p^2}\mathbf{xx} + \frac{p_y^2}{p^2}\mathbf{yy} + \mathbf{zz}\right], \quad (2)$$

where ϵ_0 is the vacuum permittivity. The description of the material properties enters via the transverse magnetic reflection coefficient, $r(\omega, p)$, which in general depends on both the frequency and, for symmetry reasons, the modulus of the wavevector $\mathbf{p}$. In a spatially local description of the material and in the near-field limit, the dependence on the wave vector disappears and the reflection coefficient is only a function of frequency [13, 16].

In order to calculate the nonequilibrium power spectrum, we model the dipole's internal dynamics as a harmonic oscillator [16]

$$\partial_t^2 \hat{\mathbf{d}}(t) + \omega_a^2 \hat{\mathbf{d}}(t) = \omega_a^2 \underline{\alpha}_0 \cdot \hat{\mathbf{E}}(\mathbf{r}_a(t), t), \quad (3)$$

where ω_a is the oscillator's frequency corresponding to the atom's characteristic dipolar resonance frequency [33], $\hat{\mathbf{E}}$ is the electric field, and $\underline{\alpha}_0$ is the static polarizability tensor, assumed to be symmetric for simplicity (it is proportional to a projector parallel to the direction of the dipole moment). We suppose that the oscillator has no intrinsic dissipation and that all the dissipative dynamics arises from the coupling to the electromagnetic field. The harmonic oscillator model allows for an analytical expression of $\underline{S}(\omega, v_x)$ given by [17]

$$\underline{S}(\omega, v_x) = \frac{\hbar}{\pi}\left[\theta(\omega)\underline{\alpha}_I(\omega, v_x) + \underline{J}(\omega, v_x)\right], \quad (4)$$

where $\theta(\omega)$ is the Heaviside-theta function. In contrast to the LTE approach which relies on the equilibrium FDT, this nonequilibrium FDT (4) contains the extra term

$$\underline{J}(\omega, v_x) = \int \frac{d^2\mathbf{p}}{(2\pi)^2}\left[\theta(\omega + p_x v_x) - \theta(\omega)\right] \times \underline{\alpha}(\omega, v_x)\cdot \underline{G}_I(\mathbf{p}, z_a, \omega + p_x v_x)\cdot \underline{\alpha}^*(\omega, v_x). \quad (5)$$

In the previous equations

$$\underline{\alpha}(\omega, v_x) = \frac{\omega_a^2}{\omega_a^2 - \Delta(\omega, v_x) - \omega^2 - \mathrm{i}\omega\gamma(\omega, v_x)}\,\underline{\alpha}_0 \quad (6)$$

is the velocity-dependent atomic polarizability, where $\gamma(\omega, v_x)$ and $\Delta(\omega, v_x)$ denote, respectively, the velocity-dependent radiative damping and frequency shift [34]

$$\frac{\Delta(\omega, v_x)}{\omega_a^2} = \int \frac{d^2\mathbf{p}}{(2\pi)^2}\mathrm{Tr}\left[\underline{\alpha}_0 \cdot \underline{G}_R(\mathbf{p}, z_a, \omega + p_x v_x)\right], \quad (7a)$$

$$\frac{\omega\gamma(\omega, v_x)}{\omega_a^2} = \int \frac{d^2\mathbf{p}}{(2\pi)^2}\mathrm{Tr}\left[\underline{\alpha}_0 \cdot \underline{G}_I(\mathbf{p}, z_a, \omega + p_x v_x)\right]. \quad (7b)$$

According to Eq. (4), the frictional force in Eq. (1) decomposes into two contributions,

$$F = F^{\mathrm{LTE}} + F^J. \quad (8)$$

The first, F^{LTE}, is what one would have obtained by applying the LTE approximation, while the second, F^J, is the correction entirely due to the nonequilibrium dynamics of the system.

Previous works [16, 17, 32, 35, 36] have shown that the quantum frictional process is characterized by a non-resonant and a resonant contribution, both being a function of the atomic velocity and the atom's separation from the surface. The resonant part occurs for sufficiently high velocities which bring the atomic transition frequency within the range of the surface plasmon-polariton resonances that exist at the vacuum/material interface. Here, we consider only the non-resonant part of the frictional force which takes place at lower velocities and is more likely to play a central role in typical experimental setups. In Appendix A we show that the main contribution to the force comes from the frequency range $0 < \omega \lesssim v_x/z_a$ (see also Refs. [16, 17]). Therefore, at sufficiently low velocities [37] the drag force is determined by the low-frequency behavior of the material's electromagnetic response. Under the assumption that the material is Ohmic for these low frequencies (we will see below that this applies to our nonlocal model), the low-velocity approximation of the LTE and the nonequilibrium contributions to the friction can be written as

(see Appendix A)

$$F^{\rm LTE} \approx -2\hbar\frac{v_x^3}{\pi}\frac{\Phi_0\Phi_2}{3}\frac{\mathcal{D}_0(z_a)\mathcal{D}_2(z_a)}{\left[1-\Delta(0,0)/\omega_a^2\right]^2}, \tag{9a}$$

$$F^{J} \approx -2\hbar\frac{v_x^3}{\pi}\Phi_1^2\frac{\mathcal{D}_1^2(z_a)}{\left[1-\Delta(0,0)/\omega_a^2\right]^2}. \tag{9b}$$

This shows that at low velocities the zero-temperature frictional force grows as the third power of the atom's velocity [8–10, 13, 14]. In the above expressions, we have introduced the abbreviations

$$\Phi_n = \binom{2n}{n}\frac{\frac{2n+1}{2(n+1)}\alpha_{xx}+\frac{1}{2(n+1)}\alpha_{yy}+\alpha_{zz}}{2^{2n+3}\pi\epsilon_0}\,, \tag{10}$$

associated with the dipole's direction in space, and

$$\mathcal{D}_n(z_a) = \int_0^\infty dp\, p^{2(n+1)}e^{-2z_a p}r_I'(0,p), \tag{11}$$

which depends on the properties of the surface (the prime indicates the first derivative with respect to the frequency). The functions $\mathcal{D}_n(z_a)$ are the $[2n]$-th derivative with respect to z_a of the low-frequency behavior of the electromagnetic density of states near the vacuum/material interface. In particular, $\mathcal{D}_0(z_a)$ is related to the atomic decay rate induced by the interaction with the radiation (radiative damping). Eqs. (9) show that, under the assumption of Ohmic dissipation, the LTE and the nonequilibrium correction have the same functional dependency on the velocity, while their behavior as a function of the distance can be distinct. In the local optics approximation, however, we have that $\mathcal{D}_0(z_a) \propto z_a^{-3}$, $\mathcal{D}_1(z_a) \propto z_a^{-5}$, and $\mathcal{D}_2(z_a) \propto z_a^{-7}$ (see Eq. (B8) in Appendix B). In this case $F^{\rm LTE}$ and F^J have the same z_a^{-10} distance dependency, as was already shown in [17].

III. THE SPATIALLY DISPERSIVE MATERIAL MODEL FOR THE METALLIC BULK

The previous results allow for a quantitative evaluation of the impact of spatial dispersion on quantum friction. At this point, we would like to recall that spatial dispersion becomes physically relevant for materials in which the free-carriers can move over distances which are much larger than the interatomic separation. This extreme mobility of charged particles is also related to collective phenomena, such as plasmon oscillations in metals [38], dynamical screening [39, 40] and quantum many-body phenomena [41]. In a macroscopic continuum description of the material, spatial dispersion leads to a nonlocal relation between the displacement and the electric fields, leading to a permittivity that depends on the wavevector of the radiation [22]. In this paper we focus on a metallic surface and describe its properties using the so-called semi-classical infinite barrier (SCIB) model [42, 43]. In this model, electrons are treated as a Fermi fluid whose dynamics is governed by the Boltzmann equation. At interfaces, electrons are assumed to be specularly reflected by an infinite potential barrier [44, 45]. Although more sophisticated models are available (see, for example, Refs. [39, 46]), the SCIB model takes into account important phenomena, such as Landau damping [47, 48], which are absent in simpler nonlocal models (e.g. the hydrodynamic model) [15, 39]. Landau damping occurs when the frequency and the wavevector of the radiation fulfill the condition $\omega \approx \mathbf{k}\cdot\mathbf{v}_p$, i.e., when the quasi-particle's velocity $\mathbf{v}_p$ becomes comparable to the phase velocity $\mathbf{v}_{ph}$ of the radiation, $v_p \sim v_{ph} = \omega/k$ ($k = |\mathbf{k}|$). Since quantum friction is very sensitive to any form of dissipation present in the system [14, 16], this intrinsic damping due to the exchange of energy between the electronic wave function and the radiation [41] will play an important role in our analysis.

Within the SCIB model, the reflection coefficient takes the form [43]

$$r(\omega,p) = \frac{1-Z(\omega,p)/Z_0(\omega,p)}{1+Z(\omega,p)/Z_0(\omega,p)}, \tag{12}$$

where $Z(\omega,p)$ is the transverse magnetic surface impedance and $Z_0(\omega,p)$ is the corresponding vacuum value. In the non-retarded limit (formally equivalent to the limit for $c\to\infty$) we have [43, 49]

$$\frac{Z(\omega,p)}{Z_0(\omega,p)} \approx \frac{2}{\pi}\int_0^\infty dq\ \frac{1}{k^2}\frac{p}{\epsilon_l(\omega,\mathbf{k})}, \tag{13}$$

such that the reflection coefficient only depends on the longitudinal part of the bulk dielectric function, $\epsilon_l(\omega,\mathbf{k})$. For the latter we use the semi-classical limit of Lindhard's quantum dielectric function [41, 42, 50]

$$\epsilon_l(\omega,\mathbf{k}) = 1+\frac{\omega_p^2}{\omega+\mathrm{i}\Gamma}\frac{3u^2 f_l(u)}{\omega+\mathrm{i}\Gamma f_l(u)}, \tag{14}$$

where Γ is the metal's dissipation rate, ω_p is the plasma frequency, the function $f_l(u)$ reads

$$f_l(u) = 1-\frac{u}{2}\ln\left[\frac{u+1}{u-1}\right], \tag{15}$$

and $u = (\omega+\mathrm{i}\Gamma)/(v_F k)$ with v_F the Fermi velocity. Equation (14) is obtained within linear response theory [41, 42, 50] by assuming a thermal equilibrium Fermi-Dirac carrier distribution. Furthermore, the expression for the permittivity is valid for wavevectors much smaller than the Fermi wavevector $k_F = m_e v_F/\hbar$ (m_e the effective electron mass) or, equivalently, when the wavelength of the radiation is much larger than the de Broglie wavelength λ_B of the electron at the Fermi surface [51–53]. Deviations from a Fermi-Dirac distribution have to be considered for strong interactions occurring at time scales shorter than the carrier equilibration time $\omega_p^{-1} \lesssim \tau_{\rm Eq} \lesssim \Gamma^{-1}$ (usually shorter than 1 ps in metals) [41, 54].

In addition, corrections to the semi-classical approach are expected for atom-surface separations $z_a \ll \lambda_B/\pi$, which for metals corresponds to half the Bohr radius, i.e., few tenths of an Ångström. As explained in section II, quantum friction is a weak low frequency phenomenon and, therefore, by considering distances $z_a > 1$ Å our approach is well within the range of validity of such a description.

Depending on the value of u, different mechanisms dominate the optical response of the metal. In the limit $|u| \to \infty$ we recover the local Drude model $\epsilon_l(\omega, k) \to \epsilon_{\rm D}(\omega) = 1 - \omega_p^2[\omega(\omega + {\rm i}\Gamma)]^{-1}$. In this case the main contributions to the atom-surface interaction stem from wavelengths $\lambda \sim 1/k$ much larger than the electron's mean free path, $\lambda \gg \ell = v_F/\Gamma$. For typical physical parameters ℓ ranges from a few tens up to a few hundreds of nanometers. Since v_F/c is of the order of the fine-structure constant, we then obtain $\ell \approx 50$ nm for a gold bulk with $\Gamma \sim 30$ meV. The local (Drude) regime corresponds to a situation where the electrons' dynamics averages over a multi-scattering scenario and their ballistic motion is negligible. In this limit the phase velocity velocity v_{ph} becomes larger than the Fermi velocity v_F, inhibiting the interaction responsible for Landau damping [41] (see also below). On the other hand, for $|u| \to 0$, the wave resolves the ballistic motion of the electron ($\lambda \ll \ell$), leading to a distinct spatially dispersive response to the electromagnetic field [22]. Scattering becomes less relevant and, since the phase velocity of the radiation is smaller or equal than the Fermi velocity, Landau damping takes over as the dominant damping mechanism. Mathematically, this phenomenon is represented by the imaginary part of the function $f_l(u)$ in the limit $|u| \to 0$ due to the logarithm appearing in Eq. (15) (see also Eq. (B2) in Appendix B).

The same physical mechanisms determine the behavior of the surface impedance. For $p\ell \ll |\omega/\Gamma + {\rm i}|$ we have $Z(\omega,p)/Z_0(\omega,p) \approx 1/\epsilon_{\rm D}(\omega)$ which leads to the usual local limit for the reflection coefficient [14]. In the limit $p\ell \gg |\omega/\Gamma + {\rm i}|$ spatial dispersion is relevant and in Appendix B we show that we can write

$$\frac{Z(\omega,p)}{Z_0(\omega,p)} \approx \frac{p\lambda_{\rm TF}}{\sqrt{1+p^2\lambda_{\rm TF}^2}} - {\rm i}\frac{\frac{\omega}{\omega_p}Q\left(p\lambda_{\rm TF}, \frac{\pi^2-4}{2\pi p\ell}\right)}{p\lambda_{\rm TF}(1+p^2\lambda_{\rm TF}^2)}, \quad (16)$$

where we have defined the function

$$Q(a,b) = \frac{a^2\left(a^2+1\right)}{\sqrt{3}}\int_0^1 dx\ \frac{1+bx}{\sqrt{1-x^2}}\frac{x^3}{(a^2+x^2)^2}. \quad (17)$$

Note that the function $Q(a,b)$ is real and nonzero also for $b = 0$, which corresponds to the limits $\ell \to \infty$ or $\Gamma \to 0$. Indeed, due to the Landau damping and despite a vanishing collision rate Γ, Eq. (16) still has a nonzero imaginary part at low frequencies, which implies a dissipative reflection coefficient. In Eq. (16) $\lambda_{\rm TF} = v_F/(\sqrt{3}\omega_p)$ is the Thomas-Fermi screening length, which is on the order of few Ångströms for typical metals [52] (see also Appendix B) and characterizes the electrostatic screening of charges in the Fermi fluid (it can be considered as the analog of the Debye length at zero temperature [52, 55]). In our system $\lambda_{\rm TF}$ is also related to spatial distribution of the electron density near the surface [56]. Within the nonlocal region, the values for which $p\lambda_{\rm TF} < 1$ correspond to electromagnetic waves that propagate with a phase velocity $v_{ph} > v_F$ in the metal. Since at zero temperature no particles exist with velocity larger than the Fermi velocity, in this region both, Landau damping and impurity scattering, are concurrent but not fully effective dissipative processes. Conversely, for $p\lambda_{\rm TF} > 1$ dissipation is dominated by the interaction between the electrons and the electromagnetic waves. From Eqs. (12) and (16) and for $v_x \ll v_F$ we have that the imaginary part of the reflection coefficient is

$$r_I(\omega,p) \approx \frac{2\frac{\omega}{\omega_p}Q\left(p\lambda_{\rm TF}, \frac{\pi^2-4}{2\pi p\ell}\right)}{p\lambda_{\rm TF}\left(\sqrt{1+p^2\lambda_{\rm TF}^2}+p\lambda_{\rm TF}\right)^2} \equiv 2\omega\epsilon_0\rho(p), \quad (18)$$

showing that the material has an Ohmic behavior and that, formally, the resistivity $\rho(p)$ depends on the wave vector when spatial dispersion is relevant. The function $\rho(p)$ grows as $|p\lambda_{\rm TF}\ln(p\lambda_{\rm TF})|$ for small wave vectors, features a maximum around $p \sim 1/(5\lambda_{\rm TF})$, and then decreases as a power law for large $p\lambda_{\rm TF}$ (see Appendix B). Importantly, at its maximum $\rho(p)$ can be more than an order of magnitude larger than the typical resistivity of a metal in the local optics description, $\rho = \Gamma/(\epsilon_0\omega_p^2)$. We show in the next Section that the previous characteristics deeply impact the distance dependency of quantum friction between an atom and a spatially dispersive metal.

IV. EFFECTS OF SPATIAL DISPERSION ON QUANTUM FRICTION

Combining Eq. (18) with Eqs. (9-11), we are able to compute the low-velocity quantum frictional force including spatial dispersion in the material's optical response. The results are presented in Fig. 1, where the force is normalized with respect to $\bar{F}^{\rm LTE}_{\rm local}$, which is the force obtained by the simultaneous use of local optics and LTE approximations (see Eq. (19) below). The normalization is chosen in order to highlight the impact of the non-LTE corrections and of the nonlocal material properties. We also perform an average over the dipole's spatial directions (denoted by the bars above the forces) and define $\alpha_0 = {\rm Tr}[\underline{\alpha}_0]/3$, which coincides with the expression of the static isotropic atomic polarizability. According to Sec. III, we can distinguish between three physically different regions of atom-surface separations.

For distances $z_a \gg \ell$, local optics is a valid description of the metal. From Eqs. (9) we recover the results for quantum friction obtained in Ref. [17] (see also the end

of the Appendix B)

$$\bar{F}^{\rm LTE}_{\rm local} \approx -\hbar\frac{189}{2\pi^3}\left(\frac{\alpha_0}{\epsilon_0}\frac{\Gamma}{\omega_p^2}\right)^2\frac{v_x^3}{(2z_a)^{10}}, \quad \frac{\bar{F}^{J}_{\rm local}}{\bar{F}^{\rm LTE}_{\rm local}} \approx \frac{29}{35}\,. \tag{19}$$

Here, for simplicity, we neglected the contribution originating from the frequency shift, which for distances $z_a \gg (\alpha_0/\epsilon_0)^{1/3}$ (few Ångströms for typical atoms) gives only a subleading contribution to the force that arises from the term $[1-\Delta(0,0)/\omega_a^2]$ in Eqs. (9).

When spatial dispersion is relevant, i.e. for separations smaller than the electron's mean free path, we can identify two distinct distance regimes. Starting with $\lambda_{\rm TF} \ll z_a < \ell$, we obtain

$$\frac{\bar{F}^{\rm LTE}}{\bar{F}^{\rm LTE}_{\rm local}} \approx \frac{\omega_p^2}{\Gamma^2}\frac{\left[\ln\left(\frac{B_0 z_a}{\lambda_{\rm TF}}\right)+\frac{C_0 z_a}{\ell}\right]\left[\ln\left(\frac{B_2 z_a}{\lambda_{\rm TF}}\right)+\frac{C_2 z_a}{\ell}\right]}{\frac{1}{7}\left(\frac{2z_a}{\lambda_{\rm TF}}\right)^2}\,, \tag{20a}$$

$$\frac{\bar{F}^{J}}{\bar{F}^{\rm LTE}_{\rm local}} \approx \frac{145}{7}\frac{\omega_p^2}{\Gamma^2}\left[\frac{\ln\left(\frac{B_1 z_a}{\lambda_{\rm TF}}\right)+\frac{C_1 z_a}{\ell}}{\frac{2z_a}{\lambda_{\rm TF}}}\right]^2\,, \tag{20b}$$

where B_n and C_n are the following numerical constants: $B_0 \approx 0.69$, $B_1 \approx 0.44$, $B_2 \approx 0.32$, $C_0 \approx 0.98$, $C_1 \approx 0.59$, and $C_2 \approx 0.42$ (see also Appendix B). We note that spatial nonlocality induces a non-algebraic change in the distance dependence of the force and, in contrast to the local optics case, the distance scalings of $\bar{F}^{\rm LTE}$ and $\bar{F}^{J}$ are different. As it was expected from the considerations regarding the system's nonequilibrium dynamics (see Sec. I), the contribution of the term $\bar{F}^{J}$ to the full frictional force is larger than in the local case, inducing a correction that reaches about 95 % rather than 80 % of the LTE contribution (see inset of Fig. 1). Importantly, the full nonequilibrium force in the nonlocal case is larger than the corresponding local counterpart calculated for values of the damping rate $\Gamma = 30$ meV and of the plasma frequency $\omega_p = 9$ eV. For both the LTE and the nonequilibrium contribution, nonlocality leads to an increase in the force that scales with ω_p^2/Γ^2 (see Eqs. (20)). Therefore, it is particularly relevant for very clean materials. The largest enhancement of roughly three orders of magnitude is reported for a distance $z_a \sim 10\lambda_{\rm TF}$ (of the order of 1 nm for typical metals; see Fig 1). This value is effectively an additional intrinsic length scale of the system which derives from the combination of geometry and material properties. It is related to the value of z_a for which the functions $p^{2(n+1)}e^{-2z_a p}$ and $r'_I(0,p)$ (see Eq. (18)) appearing in the integral defining $\mathcal{D}_n(z_a)$ have the maximum overlap. Physically speaking, $p^{2(n+1)}e^{-2z_a p}$ selects as a function of the distance z_a the parallel component of the wavevectors participating in the dissipative process in the material described by $r'_I(0,p)$. For each n this occurs at $z_a \approx 5(n+1)\lambda_{\rm TF}$. Another interesting point to note is the influence of spatial dispersion on the metal's resistivity. The magnitude of the frictional force at $z_a \sim 10\lambda_{\rm TF}$ is equivalent to that obtained via local optics but with a much larger dissipation rate of $\Gamma \sim 1$ eV. This corresponds to a ∼30 times higher resistivity, showing the relevance of spatial dispersion on quantum friction. This behavior can be understood with more detail by looking at the wavevector-dependent resistivity implicitly defined in Eq. (18): As described above, for values of $p\ell \gg 1$, $\rho(p)$ can reach values much larger than those of the local optics description.

For distances $z_a \ll \lambda_{\rm TF}$, the functional behavior of the frictional force changes once again. Although our model allows for a full mathematical characterization of the interaction in this distance range, atomic scale effects, dynamical screening and electron spill-out become relevant at such short separations (shorter than an Ångström for

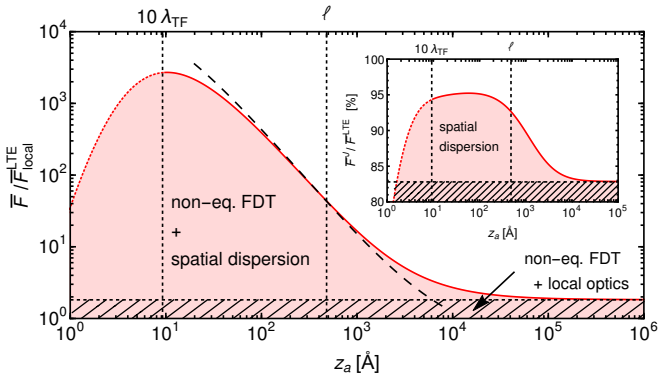

FIG. 1. Quantum frictional force acting on an atom moving at constant velocity and parallel to a metallic surface described by the SCIB model. The low-velocity limit of the force (Eqs. (9)) $\bar{F}$ is plotted as a function of the atom-surface separation z_a. In all plots, the parameters $\omega_p = 9$ eV, $\Gamma = 30$ meV, and $v_F/c = 1/137$ are fixed to these same values. In order to emphasize the role of spatial dispersion and the nonequilibrium physics, the force $\bar{F}$ is normalized to its expression obtained using local optics and the LTE approximation, $\bar{F}^{\rm LTE}_{\rm local}$. In the low-velocity regime the normalized force does not dependend on the velocity (see Eqs. (9) and (19)). For atom-surface separations much larger than the electron's mean free path $z_a \gg \ell = v_F/\gamma$, the force approaches a value which is almost twice that of $\bar{F}^{\rm LTE}_{\rm local}$, recovering the result reported in Ref. [17]. For $z_a < \ell$, spatial dispersion and the non-LTE correction result in a substantial increase of the force, with a maximum enhancement at $z_a \sim 10\lambda_{\rm TF}$, where $\lambda_{\rm TF} = v_F/(\sqrt{3}\omega_p)$ is the Thomas-Fermi screening length. The curve is dotted for distances less than 10 Å, where our description might not be reliable (see text). The black dashed line shows the total asymptotic behavior for distances $\lambda_{\rm TF} \ll z_a < \ell$ given by the sum of the expressions in Eqs. (20). The inset shows the correction exclusively due to the nonequilibrium physics, i.e. $\bar{F}^{J}/\bar{F}^{\rm LTE}$ with spatial dispersion taken into account in both forces of the numerator and the denominator. The curve shows a larger contribution of the non-LTE correction in the nonlocal case than in the local limit. It also indicates that, for the parameters used here, nonlocality is the main source of the force enhancement observed for $z_a < \ell$.

usual metals), and the continuum description of the materials is no longer reliable. For recent discussions on these topics see [57, 58]. Nevertheless, it is worth mentioning that for distances $z_a \lesssim 10\lambda_{\rm TF}$ the frictional force (denoted by the dotted line in Fig. 1) is still stronger, but increases more slowly than its local counterpart (see Fig. 1). In this case the overlap in Eq. (11) for $\mathcal{D}_n(z_a)$ selects wavevectors for which the dissipative process described by the resistivity in Eq. (18) becomes less effective.

Finally, we comment on the difference between the behavior of the frictional force for microscopic systems discussed so far, where dissipation is induced by the interaction with the electromagnetic field, and for systems where the source of dissipation is internal, like for instance in metallic nanoparticles. As pointed out in previous work [16], the LTE approximation usually provides the leading contribution to the frictional force for the latter case, for which internal dissipation is much stronger than radiative damping. Within our treatment, such systems can be described by a polarizability like in Eq. (6), but with a vanishing frequency-shift, $\Delta(\omega, v_x) = 0$ and a constant damping rate $\gamma(\omega, v_x) \equiv \gamma$. At low velocities the force is given by the relation

$$F^{\rm LTE} \approx -2\hbar \frac{v_x^3}{\pi} \frac{\Phi_2}{3} \frac{\gamma}{\omega_a^2} \mathcal{D}_2(z_a) \; . \tag{21}$$

When compared with Eq. (9a), the previous expression shows a difference in the functional dependence on the distance. In the local case this corresponds to a change in the exponent of the power law from z_a^{-10} for radiative damping to z_a^{-7} for intrinsic damping [14] (see Eq. (B8)). In the spatially dispersive case using the SCIB model, however, a more qualitative modification of the functional behavior occurs. For distances $\lambda_{\rm TF} \ll z_a < \ell$ one has

$$\frac{\bar{F}^{\rm LTE}}{\bar{F}^{\rm LTE}_{\rm local}} \approx \frac{7}{\sqrt{3}} \frac{\omega_p}{\Gamma} \frac{\ln\left[\frac{B_2 z_a}{\lambda_{\rm TF}}\right] + \frac{C_2 z_a}{\ell}}{\frac{2z_a}{\lambda_{\rm TF}}} \tag{22}$$

which shows that, in addition to a change in the power law exponent, the system with intrinsic dissipation features a single logarithm instead of the product of two logarithms as obtained in Eq. (20a) (see also Eqs. (B7) and (B8)). For such separations Eq. (21) also reveals an enhancement of the interaction due to spatial dispersion. The strengthening of the nonlocal frictional force with respect to its local counterpart has a maximum around $z_a \approx 15\lambda_{\rm TF}$. However, in the case of intrinsic dissipation, the force enhancement is less significant because $\bar{F}^{\rm LTE}/\bar{F}^{\rm LTE}_{\rm local}$ in Eq. (22) is proportional to ω_p/Γ and not to its square (see Eq. (20a)).

V. CONCLUSIONS

In the present work we investigated the impact of spatial dispersion on atom-surface quantum friction for non-relativistic velocities. Our description goes beyond the widely used local thermal equilibrium approximation and does not rely on the usual equilibrium fluctuation-dissipation theorem, but rather on an extension of it for nonequilibrium steady states [17]. The analysis focuses on the behavior of the frictional force for small velocities, which are more likely to be achieved in experimental setups. We show that for distances shorter than the electron's mean free path ℓ, spatial dispersion and the system's nonequilibrium processes have a large impact on quantum friction enhancing the interaction with respect to the LTE value. The closer the atom gets to the surface, the less important the collision-induced damping becomes and the more the Landau damping takes over as source of dissipation (see Sec. III). A maximum enhancement of three order of magnitude is attained for distances that are of the order of ten times the Thomas-Fermi screening length $\lambda_{\rm TF}$. Our results also show that in the nonlocal system the failure of the LTE approximation is more significant than in the local system, and underestimates the force by about 95 % (the nonequilibrium processes are responsible for half of the total frictional force; see the inset of Fig. 1). The inclusion of spatial dispersion does not alter the functional dependence of the interaction on the atomic velocity, which is proportional to v_x^3, but it deeply modifies its behavior as a function of the distance. Physically, this difference can be understood by recalling that the velocity dependence is related to the low frequency behavior of the electromagnetic density of states [14, 16], Ohmic for both the spatial dispersive and local materials (a sub-ohmic or a super-ohmic material will also affect the functional dependency on the velocity). Instead, the behavior as a function of the atom-surface separation is more related to the detail of the medium's optical response and to the different length scales associated with the physical processes occurring in the material. For atom-surface separations $\lambda_{\rm TF} \ll z_a < \ell$, quantum friction is no longer described by a simple power law but, due to Landau damping, it acquires a more complex structure involving a logarithmic contribution and the combination of length scales ℓ and $\lambda_{\rm TF}$ (see Eqs.(20) and (22)). In addition, unlike the local case, the contribution to the force resulting from the LTE approximation and its correction have a different distance dependence, showing again the relevance of the interplay of nonequilibrium effects and spatial dispersion for quantum frictional processes.

Quantum friction is a very weak effect and experimental investigations are therefore challenging [16]. Relatively simple time-of-flight experiments, where atoms are sent parallel to a surface and decelerations or stopping distances are measured, are possible but they may not provide the required sensitivity. Consequently, rather sophisticated atom-interferometric techniques would be better suited [59, 64]. In view of the desired atom-surface separations, such experimental designs come with their own challenges. For instance, at least one arm of the interferometer must be aligned parallel to the surface at

comparatively short distances of some tens of nanometers to the surface. The frictional force will produce a different phase accumulation in this arm with respect to a second arm being placed at much larger separations to the surface. The resulting phase shift, encoding the information on the drag force, will appear in the interference pattern. In order to exploit the enhancement effects associated with spatial nonlocality, the atom-surface separation should be of the order of or shorter than the electron mean free path ℓ in the material composing the surface (large ℓ values correspond to clean materials). While this clearly is challenging, it is not entirely out of reach. Inspecting Eqs. (19) and (20), we note that in the nonlocal region the frictional force scales in absolute value as ω_p^{-2}. According to our results, preferable characteristics of the surface material are therefore a reasonably small dissipation rate as well as plasma frequency. The latter conditions point, for example, to doped semiconductors like ZnO:Ga for which $\Gamma \sim 50$ meV and $\omega_p \sim 1$ eV have already been measured [60]. The dielectric response of highly-doped semiconductors is, however, more involved than the simple model used here and the corresponding behavior of quantum friction will be investigated in detail in future work.

VI. ACKNOWLEDGMENTS

DR thanks the CNLS for the hospitality as well as for financial support and the DAAD for funding through the PROMOS fellowship. We also acknowledge support by the LANL LDRD program, and by the Deutsche Forschungsgemeinschaft (DFG) through project B10 within the Collaborative Research Center (CRC) 951 Hybrid Inorganic/Organic Systems for Opto-Electronics (HIOS). FI further acknowledges financial support from the European Union Marie Curie People program through the Career Integration Grant No. PCIG14- GA-2013-631571 and from the DFG through the DIP program (Grant No. SCHM 1049/7-1).

Appendix A: Low-velocity expansion

In this appendix we provide the main steps of the procedure that allows to obtain the low-velocity asymptotic expressions given in Eq. (9). First of all, it is convenient to define the tensor

$$\underline{\mathcal{G}}(|p_x|, z_a, \omega) = \int_{-\infty}^{\infty} \frac{dp_y}{2\pi} \underline{G}(\mathbf{p}, z_a, \omega) \ , \qquad \text{(A1)}$$

which has the same symmetry properties as $\underline{G}(\mathbf{p}, z_a, \omega)$ with respect to the variable ω, namely an even real part and an odd imaginary part under the change $\omega \to -\omega$. Inserting Eq. (4) in Eq. (1) we can define

$$F^{\rm LTE} = -4\hbar \int_0^{\infty} \frac{dp_x}{2\pi} p_x \int_0^{p_x v_x} \frac{d\omega}{2\pi} \times \mathrm{Tr}\left[\underline{\alpha}_I(p_x v_x - \omega, v_x) \cdot \underline{\mathcal{G}}_I(|p_x|, z_a, \omega)\right] \ , \qquad \text{(A2a)}$$

$$F^{J} = -2\hbar \int_{-\infty}^{\infty} \frac{dp_x}{2\pi} p_x \int_{-\infty}^{\infty} \frac{d\omega}{2\pi} \times \mathrm{Tr}\left[\underline{J}(p_x v_x - \omega, v_x) \cdot \underline{\mathcal{G}}_I(|p_x|, z_a, \omega)\right] \ . \qquad \text{(A2b)}$$

Further manipulations of the previous expressions are possible. First, using the parity properties of $\underline{\mathcal{G}}(|p_x|, z_a, \omega)$ and treating the cases $\omega > 0$ and $\omega < 0$ separately, one can show that the expression for $\underline{J}(\omega, v_x)$ in Eq. (5) can be rewritten as (see also the Supplementary Material of Ref. [16])

$$\underline{J}(\omega, v_x) = \int_{\frac{|\omega|}{v_x}}^{\infty} \frac{dp_x}{2\pi} \times \underline{\alpha}(\omega, v_x) \cdot \underline{\mathcal{G}}_I(|p_x|, z_a, p_x v_x - |\omega|) \cdot \underline{\alpha}^*(\omega, v_x) \ . \qquad \text{(A3)}$$

The integration in Eq. (A2b) can be simplified by rearranging the integration domain as follows

$$\int_{-\infty}^{\infty} \frac{d\omega}{2\pi} \int_{\frac{|p_x v_x - \omega|}{v_x}}^{\infty} \frac{d\tilde{p}_x}{2\pi}(\ldots) = \int_0^{\infty} \frac{d\tilde{p}_x}{2\pi} \int_{p_x v_x}^{(p_x+\tilde{p}_x)v_x} \frac{d\omega}{2\pi}(\ldots) + \int_0^{\infty} \frac{d\tilde{p}_x}{2\pi} \int_{(p_x-\tilde{p}_x)v_x}^{p_x v_x} \frac{d\omega}{2\pi}(\ldots) \ . \qquad \text{(A4)}$$

Combining all the previous expressions, using the parity properties of $\underline{\mathcal{G}}(|p_x|, z_a, \omega)$ and the definition of $\gamma(\omega, v_x)$ in Eq. (7b) we have

$$F^{\rm LTE} = -4\hbar \int_0^{\infty} \frac{dp_x}{2\pi} p_x \int_{-\infty}^{\infty} \frac{d\tilde{p}_x}{2\pi} \int_0^{p_x v_x} \frac{d\omega}{2\pi} |A(p_x v_x - \omega, v_x)|^2 \times \mathrm{Tr}\left[\underline{\alpha}_0 \cdot \underline{\mathcal{G}}_I(|\tilde{p}_x|, z_a, [p_x + \tilde{p}_x]v_x - \omega)\right] \mathrm{Tr}\left[\underline{\alpha}_0 \cdot \underline{\mathcal{G}}_I(|p_x|, z_a, \omega)\right] \ , \qquad \text{(A5a)}$$

$$F^{J} = -2\hbar \int_{-\infty}^{\infty} \frac{dp_x}{2\pi} p_x \int_{-\infty}^{\infty} \frac{d\tilde{p}_x}{2\pi} \int_{p_x v_x}^{[p_x+\tilde{p}_x]v_x} \frac{d\omega}{2\pi} |A(p_x v_x - \omega, v_x)|^2 \times \mathrm{Tr}\left[\underline{\alpha}_0 \cdot \underline{\mathcal{G}}_I(|\tilde{p}_x|, z_a, [p_x + \tilde{p}_x]v_x - \omega) \cdot \underline{\alpha}_0 \cdot \underline{\mathcal{G}}_I(|p_x|, z_a, \omega)\right] \ , \qquad \text{(A5b)}$$

where we also rewrote Eq. (6) as $\underline{\alpha}(\omega, v_x) = A(\omega, v_x)\underline{\alpha}_0$. Due to the exponential function in the Green tensor in Eq. (2), the dominant wavevectors contributing to the

above integrals are $p_x \lesssim 1/z_a$. The previous expressions show that quantum friction is dominated by frequencies $\omega \lesssim v_x/z_a$. Under the assumption that for these frequencies a Taylor expansion in ω of the function $\underline{\mathcal{G}}(|p_x|, z_a, \omega)$ is possible and that $\underline{\mathcal{G}}(|p_x|, z_a, \omega) \approx \underline{\mathcal{G}}_R(|p_x|, z_a, 0) + \mathrm{i}\omega\underline{\mathcal{G}}'_I(|p_x|, z_a, 0)$ describes the relevant physics, we have

$$F^{\mathrm{LTE}} = -2\frac{v_x^3}{\pi}\hbar\left|A(0,0)\right|^2 \frac{1}{3}\int_0^\infty \frac{dp_x}{2\pi}p_x^4 \mathrm{Tr}\left[\underline{\alpha}_0 \cdot \underline{\mathcal{G}}'_I(|p_x|, z_a, 0)\right] \int_0^\infty \frac{d\tilde{p}_x}{2\pi}\mathrm{Tr}\left[\underline{\alpha}_0 \cdot \underline{\mathcal{G}}'_I(|\tilde{p}_x|, z_a, 0)\right] \ , \tag{A6a}$$

$$F^{J} = -2\frac{v_x^3}{\pi}\hbar\left|A(0,0)\right|^2 \int_0^\infty \frac{dp_x}{2\pi}p_x^2 \mathrm{Tr}\left[\underline{\alpha}_0 \cdot \underline{\mathcal{G}}'_I(|p_x|, z_a, 0)\right] \int_0^\infty \frac{d\tilde{p}_x}{2\pi}\tilde{p}_x^2\mathrm{Tr}\left[\underline{\alpha}_0 \cdot \underline{\mathcal{G}}'_I(|\tilde{p}_x|, z_a, 0)\right] \ , \tag{A6b}$$

where we also used that $\underline{\alpha}_0 = 2\mathbf{dd}/\hbar\omega_a$. The previous expressions are quite similar and they involve products of the integral

$$I_n(z_a) = \int_0^\infty \frac{dp_x}{2\pi}p_x^{2n}\mathrm{Tr}\left[\underline{\alpha}_0 \cdot \underline{\mathcal{G}}'_I(|p_x|, z_a, 0)\right] \ , \tag{A7}$$

where $n = 0, 1, 2$. Using the expression for the Green tensor given in Eq. (2), after going to polar coordinates one can show that the previous function can be written as $I_n(z_a) = \Phi_n \mathcal{D}_n(z_a)$, where Φ_n and $\mathcal{D}_n(z_a)$ are given by

$$\Phi_n = \binom{2n}{n}\frac{\frac{2n+1}{2(n+1)}\alpha_{xx} + \frac{1}{2(n+1)}\alpha_{yy} + \alpha_{zz}}{2^{2n+3}\pi\epsilon_0} \ , \tag{A8}$$

and

$$\mathcal{D}_n(z_a) = \int_0^\infty dp\, p^{2(n+1)}e^{-2z_a p}r'_I(0,p). \tag{A9}$$

Appendix B: The nonlocal impedance

In this appendix we discuss the equations reported in Sec. III. For this purpose it is convenient to define the following quantities: $\ell = v_F/\gamma$, $\lambda_{\mathrm{TF}} = v_F/(\omega_p\sqrt{3})$ and $\kappa_F = (\omega + \mathrm{i}\gamma)/v_F = \omega/v_F + \mathrm{i}/\ell$. Using these definitions we rewrite the dielectric function in Eq. (14) as

$$\epsilon_l(\kappa_F, u) = \left[1 + \frac{u^2}{\kappa_F^2\lambda_{\mathrm{TF}}^2}\right]\left[1 + \frac{u^2}{\kappa_F^2\lambda_{\mathrm{TF}}^2 + u^2}\frac{f_l(u) - 1}{1 + \mathrm{i}\frac{f_l(u)}{\kappa_F\ell - \mathrm{i}}}\right] \ , \tag{B1}$$

where $u = \kappa_F/k$. In the first factor we recognize the Thomas-Fermi dielectric function $\epsilon_{\mathrm{TF}}(k) = 1 + (k^2\lambda_{\mathrm{TF}}^2)^{-1}$ describing charge screening in the metal [52]. The additional factor is the correction introduced by the semi-classical Lindhard dielectric function [43]. As explained in the main text (see the beginning of Sec. III) the nonlocal region is characterized by $|u| \ll 1$ (low frequencies and/or large wavevectors) and therefore

$$f_l(u) = 1 + \frac{\mathrm{i}\pi u}{2} - u^2 + \mathcal{O}(u^4). \tag{B2}$$

The accuracy of the previous approximation also explains why the asymptotic behaviors presented in Eqs. (20) provide a good description also for $z_a \lesssim \ell$. In this regime the correction to the Thomas-Fermi model is small [61–63] and with the changes of variable $q \to u = x\kappa_F/p$, we can write Eq. (13) as

$$\frac{Z(p,\omega)}{Z_0(p,\omega)} \approx \frac{2}{\pi}\int_0^1 dx\ \frac{1}{\sqrt{1-x^2}}\frac{1}{\epsilon_l\left(\kappa_F, x\frac{\kappa_F}{p}\right)} \ . \tag{B3}$$

In the nonlocal region κ_F/p is small and expanding the integrand in this variable leads to

$$\frac{1}{\epsilon_l\left(\kappa_F, x\frac{\kappa_F}{p}\right)} \approx \frac{1}{1 + \frac{x^2}{p^2\lambda_{\mathrm{TF}}^2}} - \mathrm{i}\frac{\frac{\pi}{2}\frac{\omega}{\omega_p\sqrt{3}}p\lambda_{\mathrm{TF}}x^3}{(p^2\lambda_{\mathrm{TF}}^2 + x^2)^2}\left[1 + x\frac{\pi^2 - 4}{2\pi p\ell}\right] \ . \tag{B4}$$

In the above expression we have neglected a contribution $\propto \omega^2$ since for quantum friction we are interested in the low-frequency (Ohmic) region. The above expression allows for an analytical evaluation of Eq. (B3). The relevant integrals are

$$\frac{2}{\pi}\int_0^1 dx\ \frac{1}{\sqrt{1-x^2}}\frac{1}{1 + \frac{x^2}{a^2}} = \frac{a}{\sqrt{1+a^2}} \tag{B5}$$

and the integral given in Eq. (17), defining the function $Q(a,b)$. Although it results in a mathematically more involved function, this last integral can also be evaluated analytically and gives

$$\begin{aligned} Q(a,b) &= \frac{a^2}{2\sqrt{3}}\left[\frac{a^2+2}{\sqrt{a^2+1}}\ln\left(\frac{\sqrt{a^2+1}+1}{a}\right) - 1 + \left(a^2 + 1 - a\frac{a^2+\frac{3}{2}}{\sqrt{a^2+1}}\right)\pi b\right] \\ &\approx \frac{2}{\sqrt{3}}\begin{cases} -\frac{a^2}{2}\left[\ln\left(\frac{a}{2}\right) + \frac{1-\pi b}{2}\right] & a \ll 1 \\ \frac{1}{3} - \frac{1}{5a^2} + \frac{3}{32}\left(1 - \frac{2}{3a^2}\right)\pi b & a \gg 1 \end{cases} . \end{aligned} \tag{B6}$$

These results lead to Eq. (18) and allow the evaluation of the asymptotic expressions of the function $\mathcal{D}_n(z_a)$. In the nonlocal region we distinguish the cases $n = 0$ and $n = 1, 2$:

$$\mathcal{D}_0(z_a) \approx \begin{cases} \frac{4\sqrt{3}\lambda_{\rm TF}}{(2z_a)^4} \frac{\ln\left(\frac{B_0 z_a}{\lambda_{\rm TF}}\right) + \frac{C_0 z_a}{\ell}}{\omega_p} & z_a \gg \lambda_{\rm TF} \\ -\frac{1}{3\sqrt{3}\lambda_{\rm TF}^3} \frac{\ln\left(\frac{\tilde{B}_0 z_a}{\lambda_{\rm TF}}\right) - \frac{\pi z_a}{\sqrt{2}\lambda_{\rm TF}}}{\omega_p} & z_a \ll \lambda_{\rm TF} \end{cases}, \tag{B7a}$$

$$\mathcal{D}_n(z_a) \approx \begin{cases} \frac{2\lambda_{\rm TF}}{\sqrt{3}} \frac{(2n+3)!}{(2z_a)^{2n+4}} \frac{\ln\left(\frac{B_n z_a}{\lambda_{\rm TF}}\right) + \frac{C_n z_a}{\ell}}{\omega_p} & z_a \gg \lambda_{\rm TF} \\ \frac{(2n-1)!}{3\sqrt{3}\lambda_{\rm TF}^3 (2z_a)^{2n}} \frac{1}{\omega_p} & z_a \ll \lambda_{\rm TF} \end{cases}, \tag{B7b}$$

which lead to the the expression reported in Eq. (20). We defined the constants $B_n = 4\exp(\Gamma_{\rm Eu} - f_n)$, with $f_n = 7/3, 167/60, 433/140$, and $C_n = (\pi^2 - 4)/h_n$, with $h_n = 6, 10, 14$, where $\Gamma_{\rm Eu} \approx 0.58$ is the Euler constant. These are the numerical values that are reported after Eq. (20) in the main text. In addition we defined $\tilde{B}_0 = \sqrt{2}\exp\left[\Gamma_{\rm Eu}\right] \approx 2.52$.

In the local region ($z_a \gg \ell$), we obtain

$$\mathcal{D}_n(z_a) \overset{z_a \gg \ell}{\approx} 2\frac{\Gamma}{\omega_p^2} \begin{cases} \frac{2!}{(2z_a)^3} & n = 0 \\ \frac{4!}{(2z_a)^5} & n = 1 \\ \frac{6!}{(2z_a)^7} & n = 2 \end{cases}, \tag{B8}$$

which lead to the expressions in Eq. (19).

[1] R. S. Decca, D. López, E. Fischbach, G. L. Klimchitskaya, D. E. Krause, and V. M. Mostepanenko, *Precise comparison of theory and new experiment for the Casimir force leads to stronger constraints on thermal quantum effects and long-range interactions*, Ann. Phys. **318**, 37 (2005).

[2] F. Intravaia *et al.*, *Strong Casimir force reduction through metallic surface nanostructuring*, Nat. Commun. **4**, 2515 (2013).

[3] J. B. Pendry, *Shearing the vacuum - quantum friction*, J. Phys. Condes. Matter **9**, 10301 (1997).

[4] A. I. Volokitin and B. N. J. Persson, *Near-field radiative heat transfer and noncontact friction*, Rev. Mod. Phys. **79**, 1291 (2007).

[5] J. Mahanty, *Velocity dependence of the van der Waals force between molecules*, J. Phys. B At. Mol. Opt. Phys. **13**, 4391 (1980).

[6] W. L. Schaich and J. Harris, *Dynamic corrections to Van der Waals potentials*, J. Phys. F Metal Phys. **11**, 65 (1981).

[7] M. S. Tomassone and A. Widom, *Electronic friction forces on molecules moving near metals*, Phys. Rev. B **56**, 4938 (1997).

[8] A. I. Volokitin and B. N. J. Persson, *Dissipative van der Waals interaction between a small particle and a metal surface*, Phys. Rev. B **65**, 115419 (2002).

[9] G. Dedkov and A. Kyasov, *Electromagnetic and fluctuation-electromagnetic forces of interaction of moving particles and nanoprobes with surfaces: A nonrelativistic consideration*, Phys. Solid State **44**, 1809 (2002).

[10] A. A. Kyasov and G. V. Dedkov, *Relativistic theory of fluctuating electromagnetic slowing down of neutral spherical particles moving in close vicinity to a flat surface*, Nuclear Instrum. Methods B **195**, 247 (2002).

[11] S. Scheel and S. Y. Buhmann, *Casimir-Polder forces on moving atoms*, Phys. Rev. A **80**, 042902 (2009).

[12] G. Barton, *On van der Waals friction. II: Between atom and half-space*, New J. Phys. **12**, 113045 (2010).

[13] G. Pieplow and C. Henkel, *Fully covariant radiation force on a polarizable particle*, New J. Phys. **15**, 023027 (2013).

[14] F. Intravaia, R. O. Behunin, and D. A. R. Dalvit, *Quantum friction and fluctuation theorems*, Phys. Rev. A **89**, 050101(R) (2014).

[15] F. Intravaia, V. E. Mkrtchian, S. Y. Buhmann, S. Scheel, D. A. R. Dalvit, and C. Henkel, *Friction forces on atoms after acceleration*, J. Phys. Condes. Matter **27**, 214020 (2015).

[16] F. Intravaia, R. O. Behunin, C. Henkel, K. Busch, and D. A. R. Dalvit, *Non-Markovianity in atom-surface dispersion forces*, Phys. Rev. A **94**, 042114 (2016).

[17] F. Intravaia, R. O. Behunin, C. Henkel, K. Busch, and D. A. R. Dalvit, *Failure of Local Thermal Equilibrium in Quantum Friction*, Phys. Rev. Lett. **117**, 100402 (2016).

[18] J. Heinrichs, *Theory of van der Waals interactions between metal surfaces*, Phys. Rev. B **11**, 3625 (1975).

[19] R. Esquivel, C. Villarreal, and W. L. Mochan, *Exact surface impedance formulation of the Casimir force: Application to spatially dispersive metals*, Phys. Rev. A **68**, 052103 (2003).

[20] B. E. Sernelius, *Effects of spatial dispersion on electromagnetic surface modes and on modes associated with a gap between two half spaces*, Phys. Rev. B **71**, 235114 (2005).

[21] R. Esquivel-Sirvent, C. Villarreal, W. L. Mochan, A. M. Contreras-Reyes, and V. B. Svetovoy, *Spatial dispersion in Casimir forces: a brief review*, J. Phys. A Math. Gen. **39**, 6323 (2006).

[22] J. Jackson, *Classical Electrodynamics* (John Wiley and Sons Inc., New York, 1975).

[23] B. N. J. Persson and Z. Zhang, *Theory of friction: Coulomb drag between two closely spaced solids*, Phys. Rev. B **57**, 7327 (1998).

[24] A. I. Volokitin and B. N. J. Persson, *Noncontact friction between nanostructures*, Phys. Rev. B **68**, 155420 (2003).

[25] A. I. Volokitin and B. N. J. Persson, *Quantum Friction*, Phys. Rev. Lett. **106**, 094502 (2011).

[26] V. Despoja, P. M. Echenique, and M. Šunjić, *Nonlocal microscopic theory of quantum friction between parallel metallic slabs*, Phys. Rev. B **83**, 205424 (2011).

[27] V. Despoja, V. M. Silkin, P. M. Echenique, and M. Šunjić, *Influence of surface electronic structure on quantum friction between Ag(111) slabs*, Phys. Rev. B **92**, 125424 (2015).

[28] H. B. Callen and T. A. Welton, *Irreversibility and Generalized Noise*, Phys. Rev. **83**, 34 (1951).

[29] G. Barton, *Near-Field Heat Flow Between Two Quantum*

Oscillators, J. Stat. Phys. **165**, 1153 (2016).

[30] For simplicity we have assumed that the dipole's dynamics leads to a symmetric power spectrum. In this case $\underline{S}(\omega, v_x) = \underline{S}_R(\omega, v_x)$ and $\underline{S}_I(\omega, v_x) = 0$ [16]. As a consequence only the symmetric part of the Green tensor is contributing to the trace in Eq. (1). Moreover, even if the complete expression for $\underline{g}^s(\mathbf{p}, z_a, \omega)$ contains nondiagonal terms, these are odd in p_y and vanish upon integration over this variable, leaving Eq. (2) as the part of the near field scattered Green tensor relevant to quantum friction.

[31] G. Dedkov and A. Kyasov, *The relativistic theory of fluctuation electromagnetic interactions of moving neutral particles with a flat surface*, Phys. Solid State **45**, 1815 (2003).

[32] A. I. Volokitin and B. N. J. Persson, *Theory of the interaction forces and the radiative heat transfer between moving bodies*, Phys. Rev. B **78**, 155437 (2008).

[33] A single resonance dipole model for the atom provides only a qualitative description of the quantum frictional process. Further resonances would add more peaks to the atomic power spectrum. If each peak is roughly treated in terms of an independent harmonic oscillator, a multi-resonance description would therefore correspond to a sum of the expressions in (9) over the different frequencies and therefore to an enhancement of quantum friction.

[34] J. Klatt, R. Bennett, and S. Y. Buhmann, *Spectroscopic signatures of quantum friction*, Phys. Rev. A **94**, 063803 (2016).

[35] A. I. Volokitin, *Blackbody friction force on a relativistic small neutral particle*, Phys. Rev. A **91**, 032505 (2015).

[36] M. G. Silveirinha, *Optical Instabilities and Spontaneous Light Emission by Polarizable Moving Matter*, Phys. Rev. X **4**, 031013 (2014).

[37] For atoms with transition in the optical range and resistivity typical of usual metals the low-velocity approximation is valid for v_x/c less than 10^{-4} [16]. In general, however, the precise threshold into the low velocity regime is strictly related to the properties of the material composing the surface.

[38] D. Pines, *Collective Energy Losses in Solids*, Rev. Mod. Phys. **28**, 184 (1956).

[39] P. J. Feibelman, *Surface electromagnetic fields*, Prog. Surf. Sci. **12**, 287 (1982).

[40] A. Liebsch, *Dynamical screening at simple-metal surfaces*, Phys. Rev. B **36**, 7378 (1987).

[41] D. Pines and P. Nozieres, *The theory of quantum liquids Volume I: Normal Fermi Liquids* (W.A. Benjamin, Inc., New York, 1966).

[42] J. Lindhard, *On the properties of a gas of charged particles*, Kgl. Danske Videnskab. Selskab Mat.-Fys. Medd. **28**, 1 (1954).

[43] G. W. Ford and W. H. Weber, *Electromagnetic interactions of molecules with metal surfaces*, Phys. Rep. **113**, 195 (1984).

[44] K. L. Kliewer and R. Fuchs, *Collective Electronic Motion in a Metallic Slab*, Phys. Rev. **153**, 498 (1967).

[45] K. L. Kliewer and R. Fuchs, *Anomalous Skin Effect for Specular Electron Scattering and Optical Experiments at Non-Normal Angles of Incidence*, Phys. Rev. **172**, 607 (1968).

[46] F. Intravaia and K. Busch, *Fluorescence in nonlocal dissipative periodic structures*, Phys. Rev. A **91**, 053836 (2015).

[47] L. D. Landau, *On the vibrations of the electronic plasma*, J. Phys.(USSR) **10**, 25 (1946), [Zh. Eksp. Teor. Fiz.16,574(1946)].

[48] N. Van Kampen, *On the theory of stationary waves in plasmas*, Physica **21**, 949 (1955).

[49] H. R. Haakh and C. Henkel, *Magnetic near fields as a probe of charge transport in spatially dispersive conductors*, Eur. Phys. J. B **85**, 1 (2012).

[50] M. Dressel and G. Grüner, *Electrodynamics of solids: optical properties of electrons in matter* (Cambridge University Press, New York, 2002).

[51] N. D. Mermin, *Lindhard Dielectric Function in the Relaxation-Time Approximation*, Phys. Rev. B **1**, 2362 (1970).

[52] N. W. Ashcroft and N. D. Mermin, in *Solid States Physics*, edited by D. G. Crane (Harcourt College Publisher, New York, 1976).

[53] P.-O. Chapuis, S. Volz, C. Henkel, K. Joulain, and J.-J. Greffet, *Effects of spatial dispersion in near-field radiative heat transfer between two parallel metallic surfaces*, Phys. Rev. B **77**, 035431 (2008).

[54] W. S. Fann, R. Storz, H. W. K. Tom, and J. Bokor, *Electron thermalization in gold*, Phys. Rev. B **46**, 13592 (1992).

[55] G. Manfredi, *How to model quantum plasmas*, Fields Inst. Commun. **46**, 263 (2005).

[56] J. Heinrichs, *Response of Metal Surfaces to Static and Moving Point Charges and to Polarizable Charge Distributions*, Phys. Rev. B **8**, 1346 (1973).

[57] W. Zhu, R. Esteban, A. G. Borisov, J. J. Baumberg, P. Nordlander, H. J. Lezec, J. Aizpurua, and K. B. Crozier, *Quantum mechanical effects in plasmonic structures with subnanometre gaps*, Nat. Commun. **7**, 11495 (2016).

[58] S. Raza, S. I. Bozhevolnyi, M. Wubs, and N. A. Mortensen, *Nonlocal optical response in metallic nanostructures*, J. Phys. Condens. Matter **27**, 183204 (2015).

[59] A. D. Cronin, J. Schmiedmayer, and D. E. Pritchard, *Optics and interferometry with atoms and molecules*, Rev. Mod. Phys. **81**, 1051 (2009).

[60] S. Sadofev, S. Kalusniak, P. Schäfer, and F. Henneberger, *Molecular beam epitaxy of n-Zn(Mg)O as a low-damping plasmonic material at telecommunication wavelengths*, App. Phys. Lett. **102**, 181905 (2013).

[61] G. Barton, *Some surface effects in the hydrodynamic model of metals*, Rep. Prog. Phys. **42**, 963 (1979).

[62] P. Halevi, *Hydrodynamic model for the degenerate free-electron gas: Generalization to arbitrary frequencies*, Phys. Rev. B **51**, 7497 (1995).

[63] C. Kittel, *Introduction to Solid State Physics*, 7th ed. (John Wiley and Son Inc., New York, 1996).

[64] F. Impens, R. O. Behunin, C. Ccapa Ttira, and P. A. Maia Neto, *Non-local double-path Casimir phase in atom interferometers*, EPL **101**, 60006 (2013).